Available online at www.sciencedirect.com
SCIENCE DIRECT
Superlattices and Microstructures 40 (2006) 77–92
Superlattices and Microstructures
www.elsevier.com/locate/superlattices

Self-consistent Hartree method for calculations of exciton binding energy in quantum wells

V.A. Shuvayev[a], L.I. Deych[a,*], I.V. Ponomarev[b], A.A. Lisyansky[a]

[a] *Department of Physics, Queens College of the City University of New York, Flushing, NY 11367, United States*
[b] *Naval Research Laboratory, Washington, DC 20375, United States*

Received 18 January 2006; received in revised form 17 April 2006; accepted 8 May 2006
Available online 19 June 2006

Abstract

A new computationally efficient and flexible approach to calculating characteristics of excitons in quantum wells based on a self-consistent variational treatment of the electron–hole Coulomb interaction is developed. It is applied to several different quantum well materials and is shown to give much better (lower) values of exciton energies. The iterative scheme used to calculate the energies and respective wave functions is stable and rapidly convergent. The authors believe that the method can be an important computational tool in computing exciton characteristics in shallow quantum wells exceeding currently existing approaches in accuracy and efficiency. The method can also be naturally generalized for quantum wires and dots.

Keywords: Quantum well; Exciton energy; Self-consistent approach

1. Introduction

Quantum confinement of electrons and holes in quantum wells (QW) is known to increase binding energy of excitons and their oscillator strengths [1,2]. As a result, excitons in QW can be detected up to room temperature, which makes them very attractive for various optoelectronic applications. For this reason exciton related effects in quantum wells have been attracting a great deal of attention for several decades starting with the pioneering measurements of the exciton absorption by Dingle [3]. Since then, the exciton properties in semiconductor nanostructures have been the subject of numerous experimental and theoretical investigations. One of the main

* Corresponding author. Tel.: +1 718 997 3380; fax: +1 718 997 3349.
E-mail address: lev_deych@physics.qc.edu (L.I. Deych).

0749-6036/$ - see front matter
doi:10.1016/j.spmi.2006.05.002

problems attracting a great deal of attention is the accurate and effective computation of the exciton binding energy. This quantity is measured by several experimental techniques [4–6] and is the most important parameter determining the frequencies of exciton related resonances and their temperature stability. Interpretation of the experimentally obtained spectra requires such a theory of the binding energy, which, on the one hand, would be realistic and could incorporate details of semiconductor band structure, effects of mass and dielectric mismatches, etc. On the other hand, this theory should be computationally effective and flexible so that it could be easily adjustable for various types of structure and experimental situations.

Unfortunately, the problem of calculating exciton energies in a QW is untractable analytically even in the simplest model (isotropic parabolic conduction and valence bands, no valence-band mixing and dielectric and effective mass mismatches). The difficulties are caused by non-separability of the electron–hole Hamiltonian: the presence of QW potential breaks the translational invariance of the system, making it impossible to separate in-plane motion of electrons and holes from the motion in the direction of growth. Therefore, one has to resort to numerical calculations, and, by now, there have been developed several methods of numerical solution of the Schrödinger equation for QW excitons. More elaborate schemes [7] that would take into account valence band mixing and non-parabolicity effects are based on an expansion of the exciton wave function in terms of multicomponent envelope functions of electron and hole states and subsequent numerical solution of coupled integral equations in momentum space. Similar approaches based on a position-space expansion of the interband polarization operator in terms of the complete system of single-particle eigenfunctions of the one-dimensional Schrödinger equation for the quantum well potential were developed in Refs. [8–10]. The coefficients of this expansion, which represent the unknown wave functions of in-plane motion, satisfy an infinite set of coupled ordinary differential equations. Such a system is solved numerically after an appropriate basis truncation. These approaches suffer from difficulties related to the unknown errors due to basis truncation.

Other approaches that have been used to obtain many of the important results in this area are based on one or another version of the standard variational method [11–14], which, due to its transparency, provides basic physical insight into the problem. In this approach a certain form of the exciton wave function, depending on one or several variational parameters, is postulated. Usually, it is chosen in the form of a product of three terms. The first two are exact single-particle one-dimensional electron and hole wave functions describing their confined motion in the growth direction. The third term models the effects of the Coulomb interaction on the relative motion of an electron–hole pair. The accuracy of the results obtained within this type of calculation depends on the physical appropriateness of the latter term and its complexity, which is determined by the number of variational parameters. The more parameters that are introduced in the trial function, the lower the resulting exciton energy, but, of course, the more extensive the calculations. There is ample literature dealing with accurate variational numerical calculations of exciton binding energy in quantum wells [15–23]. The most advanced of them include the effects of Coulomb screening due to dielectric constant mismatch, as well as effective mass mismatch at heterojunctions and band degeneracy [14,15] but their application is usually limited to QW with relatively large confinement potentials, and their extension to more complex situations such as asymmetric wells or the presence of external fields is not straightforward.

The goal of this paper is to suggest an alternative version of the variational calculations, which has a number of important advantages over the currently existing approaches. The idea of this approach is that instead of imposing a particular functional dependence on the envelope wave function, we present it as a combination of functions of an arbitrary form, but which depend on fewer

than the total number of variables. In other words, we replace an original exact wave function with a trial one with forced separation of variables. This idea is similar to the Hartree approach to many-electron problems, where a wave function dependent on coordinates of all electrons is presented as a product of functions dependent on coordinates of single electrons [24]. Despite the formal analogy between the two approaches, we would like to emphasize that unlike the standard Hartree method, we do not deal with the separation of single-particle coordinates of identical particles. Instead we separate in-plane and in-growth-direction coordinates describing relative motion of an electron–hole pair. Therefore, the antisymmetrization of the wave function, which would result in exchange terms in the regular many particle Hartree–Fock method, is not required here. The exchange contribution to the electron–hole potential, if needed to be taken into account, should be incorporated directly in the exciton Schrödinger equation with the help of extra spin-dependent terms [25–27]. Applying the variational principle to this combination of functions with separated variables we derive a system of integro-differential equations for these functions describing both the motion of electrons and holes in the direction of confinement, and the relative two-dimensional in-plane motion of the exciton. Each of these functions is determined by effective potentials that have to be determined self-consistently. For instance, the effective potential of relative motion of the exciton in the in-plane directions is described in this treatment by the Coulomb potential averaged with the wave functions of the electron's (hole's) motion in the direction of confinement. The effective potential for the in-growth direction is also obtained by combining the initial quantum well potential with the appropriately averaged Coulomb potential.

The self-consistent approach has several advantages in comparison with the standard variational method. First of all, this method allows us to span a much larger functional space than standard variational approaches. As a result we can expect that the found energy will be lower and, hence, closer to the true value. Second, since we do not assume any particular functional form of the trial function, our method is more flexible. We can include, for instance, asymmetry or magnetic field to the Hamiltonian without any need to modify the procedure. Third, the self-consistent treatment of in-plane and perpendicular motion makes this approach applicable to situations, where regular methods fail, for instance to shallow quantum wells. In addition, the renormalization of confining potentials reveals a new effect, which cannot be obtained in the framework of the standard variational approach. The self-consistent confinement QW potential acquires a Coulomb tail, which results in accumulation of the additional excited discrete electron and hole levels in the vicinity of barrier energies. Experimentally this should manifest itself as an additional peak in the absorption spectrum near barrier band-gap frequencies caused by the Sommerfeld factor. Previous attempts to treat the Coulomb term in Hamiltonian (1) in a self-consistent manner have been made in Refs. [9,10,22,23,28–31]. More detailed comparison of our calculations with the earlier papers will be given below in Section 2, where we introduce a model used for calculations and derive general self-consistent equations. In Section 3 we present our numerical results and compare them with the results obtained by means of the standard variational approach. The last section presents the conclusions of our work. The auxiliary details of the calculations can be found in the Appendix.

2. The model

We illustrate our approach by considering a heavy (light) hole-exciton in a standard type-I symmetric quantum well. We assume parabolic dispersion laws for conduction and valence bands, and take into account the anisotropy of the latter. Throughout the paper we use effective atomic units (a.u.), in which the unit of length is the three-dimensional exciton

Bohr's radius $a_B = \hbar^2 \epsilon_w/(\mu_\perp^* e^2)$, the unit of energy is $E_B = \mu_\perp^* e^4/(\hbar^2 \epsilon_w^2) \equiv 2\Re y$, and the unit of mass is the generalized reduced electron–hole mass $\mu_\perp^*$ of in-plane motion for the well material: $1/\mu_\perp^* = 1/m_e^{*w} + 1/m_{\perp h}^{*w}$. The heavy (light) hole masses for in-plane and growth directions are expressed in terms of Luttinger parameters [32] γ_1, γ_2: $m_0/m_{\perp h}^* = (\gamma_1 \pm \gamma_2)$ and $m_0/m_{\parallel h}^* = (\gamma_1 \mp 2\gamma_2)$, m_0 is the free-electron mass. In this notation, $m_{e,h} = m_{e,h}^*/\mu_\perp^*$ and top (bottom) sign corresponds to heavy (light) hole. The z-axes of the coordinate system is set to be in the growth direction of the structure, and after a standard procedure of excluding the center-of-mass (COM) motion in the plane of layers [11,12] the effective exciton Hamiltonian can be presented in the form

$$\hat{H} = E_g + H_e + H_h + \frac{\mu_\perp^*}{\mu_\perp^*(z_e, z_h)} K_r + V_{reh}, \tag{1}$$

$$H_e = -\frac{1}{2}\frac{\partial}{\partial z_e}\frac{1}{m_e(z_e)}\frac{\partial}{\partial z_e} + U_e(z_e), \tag{2}$$

$$H_h = -\frac{1}{2}\frac{\partial}{\partial z_h}\frac{1}{m_{\parallel h}(z_h)}\frac{\partial}{\partial z_h} + U_h(z_h), \tag{3}$$

$$K_r = -\frac{1}{2}\left[\frac{\partial^2}{\partial r^2} + \frac{1}{r}\frac{\partial}{\partial r}\right], \tag{4}$$

where we took into account a mismatch between electron and hole masses in the well and the barrier, as well as a difference between their dielectric constants. Here E_g is gap energy, $r = \sqrt{(x_e - x_h)^2 + (y_e - y_h)^2}$ is the electron–hole separation in the xy plane, $U_{e,h}$ are confining potentials in the growth direction for electrons and holes, respectively, and V_{reh} is the renormalized by the dielectric mismatch Coulomb electron–hole attraction. We also assume that the ground state is isotropic in the plane of QW excluding, therefore, terms containing derivatives with respect to the azimuthal angle from the Hamiltonian.

The renormalized Coulomb potential can be obtained from the solution of the Poisson equation in a layered structure with the help of the image charges method [33,34]. Solution of the Poisson's equation for three-layer medium gives three different forms of the potential depending on whether the carriers reside inside or outside the well. For the case when both electron and hole are inside the well material, the potential is

$$V_{reh} = -\sum_{n=-\infty}^{+\infty} \frac{q^{|n|}}{\sqrt{r^2 + (nL - z_e + (-1)^n z_h)^2}} \equiv -\sum_{n=-\infty}^{+\infty} q^{|n|} W_n(r; z_e, (-1)^{1-n} z_h), \tag{5}$$

where

$$q = \frac{\epsilon_w - \epsilon_b}{\epsilon_w + \epsilon_b} \tag{6}$$

is the dielectric mismatch, L is the width of the well, and

$$W_n(r; z_1, z_2) = \frac{1}{\sqrt{r^2 + (z_1 + z_2 + nL)^2}}. \tag{7}$$

The zero-order term $W_0(r; z_e, -z_h)$ in Eq. (5) corresponds to unscreened Coulomb interaction. The analytical expressions for other configurations when one or two carriers are inside the barrier material can be found in Ref. [33].

We have omitted from Hamiltonian (1) contributions to the image charge potentials coming from the electron and the hole self-energy terms. These terms depend on $z_{e,h}$ coordinates only and have Coulomb tails at large distances. They formally appear as a diagonal part of the total electrostatic energy in a layered system [33,34]. Close inspection shows that these terms exhibit unphysical singularities at the interfaces $z = \pm L/2$, which cannot be removed within the employed model of well and barriers as dispersionless dielectric media without introducing additional phenomenological parameters. In order to renormalize these singularities one has to carry out more accurate microscopic calculations of the polarization-induced modifications of the confinement potential [15] that would take into account spatial dispersion of the dielectric constant. It is known, however, that if one would remove the singularities by phenomenologically cutting off the divergent part of the potential as in Refs. [33,34], the resulting corrections to the exciton binding energies would be of the order of 0.1 meV for typical III–V semiconductor materials [14]. These corrections are more than an order of magnitude less than corrections due to self-consistency effects discussed in this paper and can be, therefore, safely neglected.

Our calculations of exciton binding energy are based on *the self-consistent approach*, which, while based on the variational principle, is significantly different from the *standard variational method* [4,12–15]. The starting point for both methods is minimization of the energy functional $E[\Psi]$:

$$E[\Psi] = \int \Psi^* \hat{H} \Psi \mathrm{d}V = \min \tag{8}$$

with normalization condition for wave function

$$\int |\Psi|^2 \mathrm{d}V = 1. \tag{9}$$

The minimization procedure is determined by the choice of the trial wave function; this is where the two approaches differ. The trial function $\Psi(\mathbf{r}_e, \mathbf{r}_h)$ in the standard variational method is chosen within a class of functions with a predetermined analytical coordinate dependence. These functions depend on one or several variational parameters $\lambda_1, \lambda_2, \ldots, \lambda_n$. Then the total energy

$$E = E(\lambda_1, \lambda_2, \ldots, \lambda_n), \tag{10}$$

and numerical values of variational parameters can be found from minimization conditions

$$\frac{\partial E(\lambda_1, \lambda_2, \ldots, \lambda_n)}{\partial \lambda_i} = 0, \quad i = 1, 2, \ldots, n. \tag{11}$$

The success of this method depends essentially on the choice of the trial function. It must be simple enough to lend itself easily to the calculations, but at the same time its behavior must be close enough to the correct wave function in order to provide the proximity to the exact energy. The accuracy of calculations within this approach is eventually determined by the number of variational parameters introduced in the trial function.

Our self-consistent method employs a completely different approach to the choice of the trial functions. Instead of choosing a function with a particular coordinate dependence, we only assume that the dependence of this function on the electron and hole coordinates can be chosen in a completely or partially separable form. We construct an approximate entire wave function $\Psi(z_e, z_h, r)$ with the help of the unknown functions $\psi_1, \psi_2, \ldots$, where each function ψ_k depends on a lesser number of variables than the entire wave function. Considering variations of

these functions independently, we minimize energy functional, Eq. (8), with constraints given by Eq. (9) and derive as a result a system of coupled integro-differential equations for ψ_k.

In the case of a strong localization of excitons inside the quantum well (the size L of QW along z direction is smaller than the three-dimensional exciton Bohr's radius) it is reasonable to completely separate variables in the ground state trial function for the Hamiltonian (1):

$$\Psi_{self}(r, z_e, z_h) = \psi(r)\chi_e(z_e)\chi_h(z_h). \tag{12}$$

Assuming a separate normalization of each function in the product, we substitute Eq. (12) into Eq. (8). After variation of every function independently we obtain the system of coupled integro-differential equations:

$$\left[H_e + \overline{V}_e(z_e)\right]\chi_e(z_e) = E_e\chi_e(z_e), \tag{13}$$

$$\left[H_h + \overline{V}_h(z_h)\right]\chi_h(z_h) = E_h\chi_h(z_h), \tag{14}$$

$$\left[\alpha K_r + \overline{V}_r(r)\right]\psi(r) = E_X\psi(r), \tag{15}$$

where $\alpha = \langle\chi_e\chi_h|\frac{\mu_\perp}{\mu_\perp(z_e,z_h)}|\chi_e\chi_h\rangle$ is a coefficient appearing as a manifestation of the mass mismatch effect, and the effective potentials are defined as:

$$\overline{V}_r(r) = \langle\chi_e\chi_h|V_{reh}|\chi_e\chi_h\rangle, \tag{16}$$

$$\overline{V}_{e,h}(z_{e,h}) = \langle\psi\chi_{h,e}|V_{reh}|\psi\chi_{h,e}\rangle. \tag{17}$$

The angle brackets indicate the integration over two of three independent variables. As can be seen, α is identically equal to unity in the case of absence of mass mismatch effect and approaches $\mu_\perp^w/\mu_\perp^b$ with increasing width of QW.

By solving system (13)–(15) we obtain the best approximation for the entire wave function in a factorized form (12). The total energy of the system is given by Eq. (8). Averaging Eqs. (13)–(15) and adding them together one can obtain the following expression for the total energy:

$$E = \langle\Psi|\hat{H}|\Psi\rangle = E_e + E_h + E_X - \langle\chi_e|\overline{V}_e|\chi_e\rangle - \langle\chi_h|\overline{V}_h|\chi_h\rangle. \tag{18}$$

The electrostatic term describing interaction between the electron and the hole is added three times, and therefore should be subtracted twice. This subtraction results in the renormalization of the total energy due to the non-separability of the Hamiltonian. The total energy, in this case, cannot be thought of as a simple sum of the energy of the electron–hole interaction and the electron and hole confinement energies.

Equations similar to our Eqs. (13)–(15) were obtained previously in Ref. [28] from different considerations. Our derivation of these equations establishes their relation to the variational principle, and thus puts them on a more solid theoretical foundation. We also obtained these equations for a more general situation taking into account the effect of dielectric and mass mismatches. More detailed comparison of our calculations with the results of Ref. [28] will be presented in Section 3.

In order to obtain a solution for Eqs. (13)–(15) we apply the method of successive iterations. Expecting that the renormalization of the confining potentials is not very strong, we obtain the zero-order approximation by setting $\overline{V}_{e,h}^{(0)} = 0$ and solving equations

$$H_{e,h}\chi_{e,h}^{(0)}(z) = E_{e,h}^{(0)}\chi_{e,h}^{(0)}. \tag{19}$$

The calculated eigenfunctions $\chi_{e,h}^{(0)}(z_{e,h})$ are then substituted into integral (16) in order to find $\overline{V}_r^{(0)}(r)$, a zero approximation for $\overline{V}_r(r)$:

$$\overline{V}_r^{(0)}(r) = \langle \chi_e^{(0)} \chi_h^{(0)} | V_{reh} | \chi_e^{(0)} \chi_h^{(0)} \rangle. \tag{20}$$

The next step is to substitute the obtained effective potential into Eq. (15):

$$\left[\alpha K_r + \overline{V}_r^{(0)}(r) \right] \psi^{(0)}(r) = E_X^{(0)} \psi^{(0)}(r) \tag{21}$$

which describes properties of a two-dimensional electron–hole pair interacting via the effective potential $\overline{V}_r^{(0)}(r)$. This potential is the result of quantum-mechanical averaging of the Coulomb potential with zero-order wave functions $\chi_e^{(0)}$, $\chi_h^{(0)}$.

Substituting calculated zero-order wave functions $\psi^{(0)}(r)$, $\chi_{e,h}^{(0)}(z_{e,h})$ in Eq. (17) we can compute a correction to the QW electron and hole confined potentials $\overline{V}_{e,h}^{(1)}(z_{e,h})$ due to electron–hole interactions:

$$\overline{V}_{e,h}^{(1)}(z_{e,h}) = \langle \psi^{(0)} \chi_{h,e}^{(0)} | V_{reh} | \psi^{(0)} \chi_{h,e}^{(0)} \rangle. \tag{22}$$

This process is continued until potentials are self-consistent with a desired degree of accuracy. The condition of self-consistence can be presented in the following form

$$\langle \psi^{(n)} | \overline{V}_r^{(n)} | \psi^{(n)} \rangle \approx \langle \chi_e^{(n)} | \overline{V}_e^{(n)} | \chi_e^{(n)} \rangle \approx \langle \chi_h^{(n)} | \overline{V}_h^{(n)} | \chi_h^{(n)} \rangle. \tag{23}$$

The system of equations (13)–(22), including the self-consistency condition (23), represents the complete set of equations required to find the minimum value of the ground state energy of the exciton described by Hamiltonian (1) with the factorized form (12) of the trial function Ψ. The details of calculations of the effective potentials (16) and (17) are given in Appendix.

From computational point of view this scheme is very effective and reliable because at each step of iterations we only need to solve one-dimensional differential equations and carry out integrations. The self-consistency of our calculations presents also an additional significant benefit because from the speed of convergence of the procedure one can assess qualitatively to what degree a given functional dependence of the trial function is close to the exact solution. For instance, in the case of very broad or ultra-narrow quantum wells, where the exact wave function resembles a wave function of a three-dimensional exciton, the suggested separation of variables cannot represent this function too well, and one should expect a slow convergence of the iterations. On the other hand, for the wells of moderate thickness, where the quasi-two-dimensional nature of the excitons is manifested fully, the separation of variables should be a much better approximation for the exciton wave function, and our self-consistent procedure should converge much faster. Our calculations confirm this assertion.

As we already mentioned in the Introduction there have been previous attempts to treat the Coulomb term in Hamiltonian (1) in a self-consistent manner. For instance, in Ref. [31] and Refs. [22,23] a self-consistent treatment was used to compute the single-particle wave functions. However, for calculation of the radial, “excitonic”, part of the wave function the “traditional” non-self-consistent variational method was employed. Unlike those earlier papers, in our calculations we extend self-consistent treatment to all three factors of the trial function, carrying out, therefore, fully self-consistent calculations.

Table 1
Parameters of the materials used in the calculations: gap energy (E_{gap}), conduction band offset ($\Delta E_c/\Delta E_g$), Luttinger parameters (γ_1 and γ_2), effective mass of the electron in conduction band (m_e^*), dielectric constant (ϵ), and units of length (a_B) and energy (E_B)

Material	E_{gap} (eV)	$\Delta E_c/\Delta E_g$	γ_1	γ_2	m_e^* (m_0)	ϵ	q	a_B (Å)	E_B (meV)
GaAs	1.518	60%	6.85	2.1	0.0665	12.53	0.043	159	7.23
$Al_{0.4}Ga_{0.6}As$	2.163		4.67	1.17	0.0895	11.5			
$In_{0.53}Ga_{0.47}As$	0.813	40%	11.0	4.18	0.041	13.9	0.049	291	3.56
InP	1.423		5.15	0.94	0.0803	12.6			

a_B and E_B are given only for the well materials. Luttinger parameters correspond to the heavy-hole effective mass. All material parameters are taken from Ref. [34].

3. Discussion of results

In this section, we present the results of our calculations and compare them with the results of the standard variational method for the shallow quantum wells. The calculations were performed for two different material systems: $GaAs/Al_{0.4}Ga_{0.6}As$ and $In_{0.53}Ga_{0.47}As/InP$, which have been extensively studied in the past so that our calculations can be compared with previous results. The concrete parameters of these structures used in our calculations are listed in Table 1. The mismatch of the dielectric constants has been taken into account by truncating infinite sums in the effective potential Eq. (5) at the terms of the order of q^5. Given the values of the mismatch parameter q for the studied systems this approximation was found to be sufficient to provide the exciton binding energies with desirable accuracy.

We begin discussing the results of our calculations by considering the evolution of the effective potential $\overline{V}_e(z_e)$ from one iterative step to another. This potential is a Coulomb induced modification to the rectangular shape well $U_e(z_e)$ [see Eq. (2)]. Initially it sets to zero, but subsequent iterations result in significant modification of its shape. Fig. 1 shows an example of the evolution of this potential in the case of a heavy-hole exciton in a $GaAs/Al_{0.4}Ga_{0.6}As$ 120 Å wide single quantum well. One can see from the presented plots that the most changes in the shape of the effective potential occur only at the first three iteration steps. Subsequent iterations result only in minor modifications of the potential and the position of the single-particle one-dimensional energy level until Eq. (23) is satisfied. Similar modification occurs with the hole "single-particle" potential $\overline{V_h(z_h)}$.

The main result of these modifications is a downshift of the effective "single-particle" contributions to the total exciton energy. There is an additional non-trivial effect also. As a result of the self-consistent contributions, both electron and hole effective potentials acquire a long "Coulomb-like" tail at large values of z: $\overline{V_{e,h}(z_{e,h})} \sim 1/z_{e,h}$. This renormalization significantly modifies the spectrum of "single-particle" effective energies bringing an additional number of excited discrete energy levels extending from the single-particle ground states up to the height of the barrier. An example of these modifications is shown in Fig. 2 for the conduction band of a 45 Å wide $GaAs/Al_{0.4}Ga_{0.6}As$. One can see a significant lowering of the ground state energy of the electron after the fourth iteration of the self-consistent procedure compared to its non-self-consistent initial value. Also shown (schematically) are new energy levels arising due to the renormalization of the potential. It should be noted, however, that the conclusion about the appearance of these new excited levels has to be approached with caution. Indeed, the variational procedure is designed for calculations of the energy of the ground state, and use of the variational procedure to study excited states in the modified potential is not fully justified. One

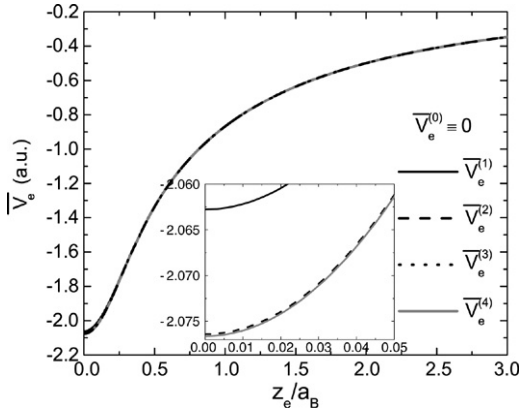

Fig. 1. Evolution of the effective potential $\overline{V}_e(z_e)$ with every step of successive approximation for a HH exciton in a GaAs/$Al_{0.4}Ga_{0.6}$As 120 Å single quantum well. Calculations are taking into account both mass and dielectric mismatches. Due to the symmetry of the potential only one half of it is shown on the graph. Solid, dashed, dotted and solid gray lines represent effective potential at the first four consecutive iterations correspondingly.

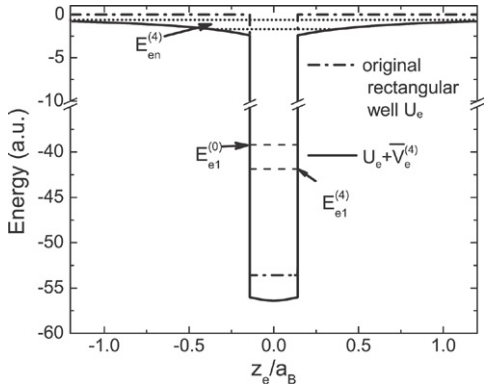

Fig. 2. Modification of the conduction band of a HH exciton in a GaAs/$Al_{0.4}Ga_{0.6}$As 45 Å single quantum well due to the presence of the effective potential. The dashed dotted line presents initial profile of the conduction band and the solid line is its configuration at the fourth step. $E_{e1}^{(0)}$ and $E_{e1}^{(4)}$ show the position of the electron ground state energy in initial and modified potentials. $E_{en}^{(4)}$ are the new excited levels of the electron appearing due to the renormalization of the conduction band. These levels were not calculated and their positions are shown schematically. Valence band profile and the value of the hole's ground state energy are modifying in the same way.

can still calculate excited states using this approach carrying out self-consistent adjustments of the effective potential for each new excited level. While this question requires a separate analysis, which lies outside of the scope of this paper, we would like to mention that qualitatively these excited levels would manifest themselves as a modification of the absorption spectrum in the vicinity of the barrier band-gap energy. Such a modification was possibly observed in Ref. [35] on an absorption spectrum of narrow quantum wells. This issue was also discussed in Ref. [28], where the energies of the excitonic transitions between excited electron and hole levels were obtained from the photoluminescence spectra in the presence of the magnetic field.

Fig. 3 presents the evolution of the excitonic effective potential $\overline{V}_r(r)$ with the iterations. Because of the singular behavior of the potential at $r = 0$, which results in large values of the

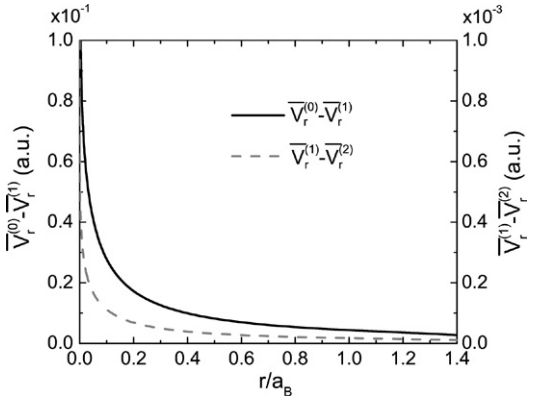

Fig. 3. Changes in the effective potential $\overline{V}_r(r)$ with every step of successive approximation for a HH exciton in a $GaAs/Al_{0.4}Ga_{0.6}As$ 50 Å single quantum well. The solid curve represents a difference between the value of the potential at a zero and first iterations, while the dashed line shows the difference between first and second iterations. In order to distinguish the latter curve from zero it was plotted with its own scale presented on the right-hand axes of the plot.

Table 2
Effective parameters describing a HH exciton in $GaAs/Al_{0.4}Ga_{0.6}As$ 20 Å single quantum well calculated at several steps of the iteration procedure

n	$-E_X$	$-E_e$	$-E_h$	$\langle R\rangle$	$\langle z_e^2\rangle$	$\langle z_h^2\rangle$	$\langle\overline{V}_e\rangle$	$\langle\overline{V}_h\rangle$	$\langle\overline{V}_r\rangle$
0	1.75414	22.24994	23.87359	0.563147	0.006626	0.002002	0.00000	0.00000	3.06164
1	1.75631	25.31296	26.93540	0.562744	0.006476	0.001988	3.06436	3.06197	3.06697
2	1.75632	25.31557	26.94040	0.562748	0.006476	0.001988	3.06698	3.06697	3.06698
3	1.75632	25.31557	26.94041	0.562741	0.006476	0.001988	3.06698	3.06698	3.06698

The first column presents the number of the iteration, other columns — binding energy E_X, electron (hole) energy $E_e(E_h)$, average radius of the exciton in well's plane $\langle R\rangle$, average of z_e^2 and z_h^2, average effective potentials $\overline{V}_e$, $\overline{V}_h$, and $\overline{V}_r$, respectively. All energies are in terms of energy units and all lengths are in terms of length units of the well material. In our case it is more convenient to count energies from the barrier band edge rather than from the bottom of the well.

potential at small r, the relative changes of the potential can hardly be seen directly. Therefore, we present here differences between values of the potential at several consecutive iterations. One can see that the largest change occurs at the first iteration (left axes of the plot), while other consecutive iterations (right axes) result in much smaller modifications. While relative renormalization of this potential resulting from the self-consistent treatment is not very large, we will show that it results in quite significant corrections to the exciton binding energy, which justifies the necessity of complete self-consistent treatment for accurate calculations of the binding energy.

Changes of the most important effective parameters of the system with iterations for a heavy-hole exciton in a 20 Å wide $GaAs/Al_{0.4}Ga_{0.6}As$ single quantum well structure are shown in Table 2. This table confirms the original conclusion based on Fig. 1 that main changes occur only at the first three iterations.

In order to compare our method with the standard variational approach we calculated the dependence of the binding energy of the heavy-hole exciton in $GaAs/Al_{0.4}Ga_{0.6}As$ and $In_{0.53}Ga_{0.47}As/InP$ structures on the width of the quantum well. These calculations are compared with the results obtained by a standard variational method in Ref. [34]. The authors of that work

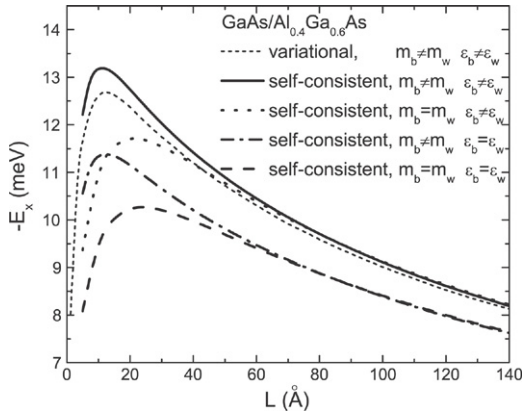

Fig. 4. Dependence of the binding energy of a HH exciton in a $GaAs/Al_{0.4}Ga_{0.6}As$ single quantum well on the width of the well. Curves represent different parameters of the well and barrier materials with and without mass mismatch (*mm*) and dielectric mismatch (*dm*): *mm* and *dm* (solid line), only *dm* (dotted line), only *mm* (dashed dotted line) and dashed line does not have any mismatch. Comparison with the results of the standard variational approach (short dashed line) is based on data taken from Ref. [34] and includes both mismatches.

calculated binding energy using a trial function with two variational parameters:

$$\phi(\rho, z_e, z_h) = \exp\left(-\frac{1}{a}\sqrt{\rho^2 + \lambda^2(z_e - z_h)^2}\right) u_e(z_e) u_h(z_h), \tag{24}$$

where $u_{e,h}(z_{e,h})$ are single-particle one-dimensional wave functions describing confinement of the electrons and holes in the well. The results obtained by this approach included both mass and dielectric mismatches, which were introduced much in the same way as in our paper with one exception. The authors of Ref. [34] included self-energy terms describing interaction of electrons and holes with their own images and concluded that these terms do not effect exciton energies in the materials under consideration in any significant way. Based on this conclusion we believe that it is reasonable to compare our results with those of Ref. [34] even though we have omitted the self-energy terms from our Hamiltonian.

In Figs. 4 and 5 we have plotted the dependence of the binding energy of a heavy-hole exciton in $GaAs/Al_{0.4}Ga_{0.6}As$ and $In_{0.53}Ga_{0.47}As/InP$ structures as a function of well width for several different assumptions regarding the mass and dielectric mismatches: without any mismatches, with mass or dielectric mismatch only, and with both mismatches taken into account simultaneously. This analysis allows us not only to compare our own and standard variational approaches, but also to assess effects of various discontinuities on the exciton energy. In all approximations we obtain a well known non-monotonic dependence of the binding energy on the well width with a maximum at its intermediate value. Comparing the plotted curves, however, we see that different types of discontinuities affect the energy differently. For instance, we can see that the mismatch of dielectric constants doesn't change the shape or position of the maximum of the dependence. It, however, shifts up the value of the binding energy even for relatively wide quantum wells, where excitons should be totally confined in the well's region.

The mass mismatch across the well–barrier interface produces a qualitatively different effect. The form of the dependence of the binding energy on width significantly changes only at well widths comparable with the exciton Bohr radius. In this case the maximum of the curve shifts toward smaller values of the width and its shape becomes steeper close to it. Sum of these two

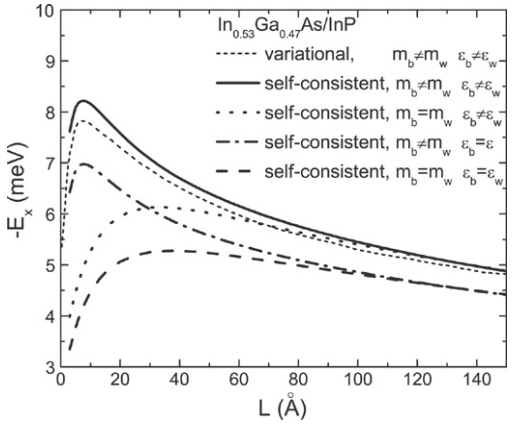

Fig. 5. Dependence of the binding energy of a HH exciton in a $In_{0.53}Ga_{0.47}As/InP$ single quantum well on the width of the well. Curves represent different parameters of the well and barrier materials with and without mass mismatch (*mm*) and dielectric mismatch (*dm*): *mm* and *dm* (solid line), only *dm* (dotted line), only *mm* (dashed dotted line) and dashed line does not have any mismatch. Comparison with the results of the standard variational approach (short dashed line) is based on data taken from Ref. [34] and includes both mismatches.

effects results in the increase of binding energy by up to 30% at the maximum, while shifting its position to smaller widths compared to the case without any mismatch. Finally, comparing the results of our calculations with those of the standard variational approach one can see that our method gives better (meaning lower) values for the exciton energy for the entire considered range of quantum well thicknesses and for both considered material systems.

It is interesting to compare our calculations with the results of Ref. [28], where the same self-consistent equations were solved but without taking into account dielectric and mass mismatches. The $GaAs/Al_{0.05}Ga_{0.95}As$ quantum well structure studied in Ref. [28] can be characterized by the following values of the parameters of GaAs: $m_e = 0.0665m_0$, $\gamma_1 = 6.79$, $\gamma_2 = 1.924$ and $\epsilon = 12.5$; the band offset at the heterojunction is 81.1 meV with its distribution between the conduction band and the valence band 62% and 38% respectively. The authors of that work neglected a difference between parameters of the well and the barrier material due to the low content of the Al in the latter. In order to clarify the role of the mismatch in this case we obtained parameters for $Al_{0.05}Ga_{0.95}As$ using a linear interpolation between GaAs and $Al_{0.4}Ga_{0.6}As$. In order to find the Luttinger parameters the interpolation was applied to masses $m^*_{\perp h}$ and $m^*_{\parallel h}$ of the respective materials. This procedure resulted in the following values for the material parameters of the barrier layer: $m_e = 0.06937m_0$, $\gamma_1 = 6.422$, $\gamma_2 = 1.787$ and $\epsilon = 12.4$.

The results of our calculations are presented in Fig. 6, which shows the energy (10) minus the band gap in the barrier layer as a function of the width of the well. The insert represents the calculated difference in energy of the excitonic transition between the system with dielectric and mass mismatches and the one without them. These figures show that even such a small mismatch makes an appreciable contribution to the exciton energy. We also have to notice that even without the mismatch our calculations differ from the results of Ref. [28] for wider wells. The origin of this discrepancy cannot be ascertained at the present time because of the lack of details of the computational procedure used in Ref. [28].

Fig. 7 represents the dependence of the excitonic oscillator strength, proportional to the $|\psi(0)|^2|\int_{-\infty}^{\infty}\chi_e(z)\chi_h(z)\mathrm{d}z|^2$, as a function of the quantum well width. The solid line shows the results of our calculations including all mismatches and the dashed line is the results taken

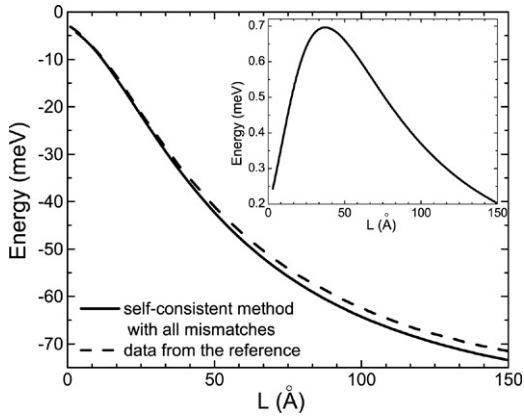

Fig. 6. Energy of excitonic transition of a HH exciton in a GaAs/$Al_{0.05}Ga_{0.95}$As single quantum well as a function of the quantum well width. Curves compare the results of our calculations with mass and dielectric mismatches taken into account (solid line) with the results from the Ref. [28] which don't have any mismatch (dashed line). The insert shows the difference of the calculated energy of excitonic transition between the system with mismatches and without them.

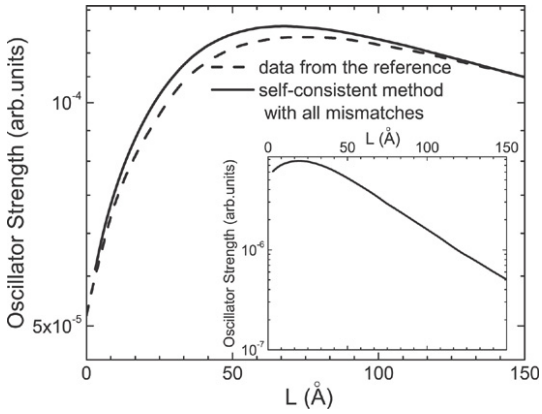

Fig. 7. Oscillator strength of excitonic transition of a HH exciton in a GaAs/$Al_{0.05}Ga_{0.95}$As single quantum well as a function of the quantum well width. Curves compare the results of our calculations with mass and dielectric mismatches taken into account (solid line) with the results from Ref. [28] which don't have any mismatches (dashed line). The insert shows the difference of oscillator strengths between the system with mismatches and without them.

from Ref. [28]. The graph on the insert is the calculated difference between the system with mismatches and without them. The introduced mismatches are enhancing the oscillator strength in the region of the quantum well widths up to 120 Å. This effect is due to stronger localization of the electron and hole wave functions inside the well in the presence of the mismatches as was described earlier in our paper.

4. Conclusions

In this work we presented a new method for calculating the exciton binding energy in a single quantum well, and demonstrated it on two different quantum wells. Our calculations showed that the suggested method gives a lower, and hence, more accurate, value of the exciton energy than

traditional variational approaches. Among other advantages of our approach is its versatility (the method can be immediately applied to more complex situations such as asymmetrical quantum wells, wells in external fields, etc.), and computational efficiency and accuracy. Besides providing more accurate values for binding energies, our approach also predicted certain modifications in the absorption spectrum of quantum wells, which can be (and maybe were) observed experimentally. This modification results from renormalization of confining electron and hole potentials due to self-consistent treatment of the Coulomb interaction.

Appendix. Expressions for the effective potentials

Choosing the origin of the coordinate system at the center of the QW the expression for effective potential $\overline{V}_r(r)$, which takes into account discontinuity of the dielectric constant [33] in the following form:

$$\overline{V}_r(r) = -[V_1(r) + V_2(r) + V_3(r)], \tag{A.1}$$

where

$$\begin{aligned}
V_1(r) &= \int_0^{L/2}\int_0^{L/2} \mathrm{d}z_e\,\mathrm{d}z_h\, F(z_e,z_h) \sum_{n=-\infty}^{\infty} q^{|n|}\{W_n(r;z_e,-z_h) + W_n(r;z_e,z_h)\},\\
V_2(r) &= 2(1+q)\int_0^{L/2}\int_{L/2}^{\infty} \mathrm{d}z_e\,\mathrm{d}z_h\, F(z_e,z_h) \sum_{n=0}^{\infty} q^{n}\{W_n(r;z_e,-z_h) + W_n(r;z_e,z_h)\},\\
V_3(r) &= \int_{L/2}^{\infty}\int_{L/2}^{\infty} \mathrm{d}z_e\,\mathrm{d}z_h\, F(z_e,z_h) \left\{ \frac{(1+q)}{(1-q)}(W_0(r;z_e,-z_h) - qW_{-1}(r,z_e,z_h)) \right.\\
&\quad \left. + (1+q)^2 \sum_{n=0}^{\infty} q^n W_n(r;z_e,z_h) \right\},
\end{aligned} \tag{A.2}$$

and

$$F(z_e,z_h) = \chi_e^2(z_e)\chi_h^2(z_h) + \chi_e^2(z_h)\chi_h^2(z_e). \tag{A.3}$$

The integrand in the effective potential (A.1) has a singularity at $r = 0, z_e = z_h$, therefore we apply a coordinate transformation $\xi = z_e - z_h, \eta = z_e + z_h$, which allows for extracting the divergent part and significantly increasing computational efficiency of the calculations. In new coordinates the potential takes the following form:

$$\begin{aligned}
V_1(r) &= \sum_{n=-\infty}^{\infty} q^{|n|} \int_0^{L/2} \mathrm{d}\eta\\
&\quad \times \left[W_{-n}(r;\eta) \int_0^{\eta} \mathrm{d}\xi\ \Phi(\xi,\eta) + W_{n-1}(r;\eta) \int_0^{\eta} \mathrm{d}\xi\ \Phi(\xi,-\eta+L) \right.\\
&\quad \left. + W_n(r;\eta) \int_{\eta}^{L-\eta} \mathrm{d}\xi\ \Phi(\eta,\xi) \right],\\
V_2(r) &= (1+q)\sum_{n=0}^{\infty} q^n (V_{21n}(r) + V_{22n}(r)),
\end{aligned}$$

$$
\begin{aligned}
V_{21n}(r) &= \int_0^{L/2} \mathrm{d}\eta \\
&\quad \times \Bigg[W_n(r;\eta) \int_0^{\eta} \mathrm{d}\xi \, (\Phi(\eta, \xi + L) + \Phi(\eta, -\xi + L)) + W_{n+\frac{1}{2}}(r;\eta) \int_0^{\eta} \mathrm{d}\xi \\
&\quad \times \left(\Phi\left(\xi + \frac{L}{2}, \eta + \frac{L}{2}\right) + \Phi\left(-\xi + \frac{L}{2}, \eta + \frac{L}{2}\right)\right)\Bigg], \\
V_{22n}(r) &= \int_{L/2}^{\infty} \mathrm{d}\eta \left[W_{n+\frac{1}{2}}(r;\eta) \int_0^{L/2} \mathrm{d}\xi \left(\Phi\left(\xi + \eta, \eta + \frac{L}{2}\right)\right.\right. \\
&\quad \left. + \Phi\left(-\xi + \eta, \eta + \frac{L}{2}\right)\right) W_n(r;\eta) \int_0^{L/2} \mathrm{d}\xi \left(\Phi\left(\eta, \xi + \eta + \frac{L}{2}\right)\right. \\
&\quad \left.\left. + \Phi\left(\eta, -\xi + \eta + \frac{L}{2}\right)\right)\right], \\
V_3(r) &= \frac{(1+q)}{(1-q)} \int_0^{\infty} \mathrm{d}\eta \left[W_0(r;\eta) \int_{\eta}^{\infty} \mathrm{d}\xi \; \Phi(\eta, \xi + L) + W_1(r;\eta) \right. \\
&\quad \times \int_0^{\eta} \mathrm{d}\xi \; \Phi(\xi, \eta + L) + \sum_{n=1}^{\infty} q^n \, (W_{n+1}(r;\eta) - W_{n-1}(r;\eta)) \\
&\quad \left. \times \int_0^{\eta} \mathrm{d}\xi \; \Phi(\xi, \eta + L)\right], \qquad \text{(A.4)}
\end{aligned}
$$

where we substituted $W_n(r;\eta) \equiv W_n(r; z_e, z_h)$ and

$$
\Phi(\xi, \eta) = F\left(\frac{\xi + \eta}{2}, \frac{\eta - \xi}{2}\right). \qquad \text{(A.5)}
$$

To treat the singularity in $V_{1,2}(r)$ we split the outer integral into two parts: $\int_0^{L/2} \mathrm{d}\eta = \int_0^{\delta} \mathrm{d}\eta + \int_{\delta}^{L/2} \mathrm{d}\eta$, with $\delta \ll 1$. For the first part the inner integral of $\Phi(\xi, \eta)$ can be replaced by the first few terms of its series expansion near $\eta = 0$. It results in the following approximation $\int_0^{\delta} \mathrm{d}\eta \, W_n(r, \eta)(y_0 + \alpha\eta + \beta\eta^2)$. Parameters y_0, α, β are the parameters of the quadratic spline. This integral can be found explicitly and it has a logarithmic divergence at small r.

The effective potentials $\overline{V}_{e,h}(z_{e,h})$ in z-directions are free from divergencies. They can be written down as follows:

$$
\overline{V}_{e,h}(z_{e,h}) = \begin{cases} V_{e,h}^{(<)}(z_{e,h}), & \text{for } z_{e,h} \le \dfrac{L}{2}, \\ V_{e,h}^{(>)}(z_{e,h}), & \text{for } z_{e,h} \ge \dfrac{L}{2}, \end{cases} \qquad \text{(A.6)}
$$

where

$$
\begin{aligned}
V_{e,h}^{(<)}(z_{e,h}) &= \int_0^{\infty} \mathrm{d}r \, r\psi^2(r) \left(\int_0^{L/2} \mathrm{d}z_{h,e} \, \chi_{h,e}^2(z_{h,e}) \sum_{n=-\infty}^{\infty} q^{|n|} (W_n(r; z_{e,h}, -z_{h,e}) \right. \\
&\quad + W_n(r; z_{e,h}, z_{h,e})) + \int_{L/2}^{\infty} \mathrm{d}z_{h,e} \, \chi_{h,e}^2(z_{h,e})(1+q) \sum_{n=0}^{\infty} q^n \\
&\quad \left. \times \; (W_n(r; z_{h,e}, -z_{e,h}) + W_n(r; z_{h,e}, z_{e,h}))\right),
\end{aligned}
$$

$$V_{e,h}^{(>)}(z_{e,h}) = \int_0^\infty \mathrm{d}r\, r\psi^2(r) \left(\int_0^{L/2} \mathrm{d}z_{h,e}\, \chi_{h,e}^2(z_{h,e})(1+q) \sum_{n=0}^{\infty} q^n (W_n(r; z_{e,h}, -z_{h,e}) + W_n(r; z_{e,h}, z_{h,e})) + \int_{L/2}^\infty \mathrm{d}z_{h,e}\, \chi_{h,e}^2(z_{h,e}) \left[(1+q)^2 \sum_{n=0}^{\infty} q^n \times W_n(r; z_{e,h}, z_{h,e}) + \frac{(1+q)}{(1-q)} (W_0(r; z_{e,h}, -z_{h,e}) - q\, W_{-1}(r; z_{e,h}, z_{h,e})) \right] \right). \quad \text{(A.7)}$$

References

[1] P. Harrison, Quantum Wells, Wires, and Dots: Theoretical and Computational Physics, John Wiley and Sons, Chichester, 1999.
[2] E. Burstein, C. Weisbuch (Eds.), Confined Electrons and Photons: New Physics and Applications, Plenum Press, New York, 1995.
[3] R. Dingle, W. Wiegmann, C.H. Henry, Phys. Rev. Lett. 33 (1974) 827.
[4] R.C. Miller, A.C. Gossard, G.D. Sanders, L.C. Chang, J.N. Schulman, Phys. Rev. B 32 (1985) 8452.
[5] R. Cingolani, P. Prete, D. Greco, P.V. Giugno, M. Lomascolo, R. Rinaldi, L. Calcagnile, L. Vanzetti, L. Sorba, A. Franciosi, Phys. Rev. B 51 (1995) 5176.
[6] T. Vanhoucke, M. Hayne, M. Henini, V.V. Moshchalkov, Phys. Rev. B 63 (2001) 125331.
[7] R. Winkler, Phys. Rev. B 51 (1995) 14395.
[8] A. Stahl, I. Balslev, Electrodynamics of the Semiconductor Band Edge, Springer, Berlin, 1987.
[9] I. Balslev, R. Zimmermann, A. Stahl, Phys. Rev. B 40 (1989) 4095.
[10] D. Merbach, E. Schöll, W. Ebeling, P. Mitchelm, J. Gutowski, Phys. Rev. B 58 (1998) 10709.
[11] R.C. Miller, D.A. Kleinman, W.T. Tsang, A.C. Gossard, Phys. Rev. B 24 (1981) 1134.
[12] G. Bastard, E.E. Mendez, L.L. Chang, L. Esaki, Phys. Rev. B 26 (1982) 1974.
[13] R.L. Greene, K.K. Bajaj, D.E. Phelps, Phys. Rev. B 29 (1984) 1807.
[14] L.C. Andreani, A. Pasquarello, Phys. Rev. B 42 (1990) 8928.
[15] B. Gerlach, J. Wusthoff, M.O. Dzero, M.A. Smondyrev, Phys. Rev. B 58 (1998) 10568.
[16] R.C. Iotti, L.C. Andreani, Phys. Rev. B 56 (1997) 3922.
[17] J. Kossut, J.K. Furdyna, M. Dobrowolska, Phys. Rev. B 56 (1997) 9775.
[18] P. Harrison, T. Piorek, W.E. Hagston, T. Stirner, Superlatt. Microstruct. 20 (1996) 45.
[19] S. de Leon, B. Laikhtman, Phys. Rev. B 61 (2000) 2874.
[20] U. Ekenberg, M. Altarelli, Phys. Rev. B 35 (1987) 7585.
[21] S.K. Chang, A.V. Nurmikko, J.W. Wu, L.A. Kolodziejski, R.L. Gunshor, Phys. Rev. B 37 (1988) 1191.
[22] J. Warnock, B.T. Jonker, A. Petrou, W.C. Chou, X. Liu, Phys. Rev. B 48 (1993) 17321.
[23] T. Piorek, P. Harrison, W.E. Hagston, Phys. Rev. B 52 (1995) 14111.
[24] D.R. Hartree, Proc. Camb. Philos. Soc. 24 (1928) 89.
[25] G.L. Bir, G.E. Pikus, Symmetry and Strain-Induced Effects in Semiconductors, Wiley, New York, 1975.
[26] Y. Chen, B. Gil, P. Lefebvre, H. Mathieu, Phys. Rev. B 37 (1988) 6429.
[27] L.C. Andreani, F. Bassani, Phys. Rev. B 41 (1990) 7536.
[28] E.A. Mulyarov, N.N. Sibel'din, M.L. Skorikov, V.A. Tsvetkov, B. Etienne, JETP Lett. 70 (1999) 621.
[29] A.L. Efros, Sov. Phys. Semicond. 20 (1986) 808.
[30] H. Castella, J.W. Wilkins, Phys. Rev. B 58 (1998) 16186.
[31] F.V. Kyrychenko, S.M. Ryabchenko, Yu.G. Semenov, Physica E 8 (2000) 275.
[32] J.C. Hensel, G. Feher, Phys. Rev. 129 (1963) 1041.
[33] M. Kumagai, T. Takagahara, Phys. Rev. B 40 (1989) 12359.
[34] D.B. Tran Thoai, R. Zimmermann, M. Grundmann, D. Bimberg, Phys. Rev. B 42 (1990) 5906.
[35] V. Voliotis, R. Grousson, P. Lavallard, R. Planel, Phys. Rev. B 52 (1995) 10725.